

CLIMATE VARIABILITY AND CHANGE SINCE 850 CE

An Ensemble Approach with the Community Earth System Model

BY BETTE L. OTTO-BLIESNER, ESTHER C. BRADY, JOHN FASULLO, ALEXANDRA JAHN, LAURA LANDRUM, SAMANTHA STEVENSON, NAN ROSENBLOOM, ANDREW MAI, AND GARY STRAND

The Community Earth System Model-Last Millennium Ensemble (CESM-LME) modeling project gives the research community a resource for better understanding both proxy records and climate variability and change since 850 CE.

In 1565, Pieter Bruegel the Elder painted the frigid northern European landscape in his work *Hunters in the Snow*, one of a series of winter landscape paintings (Kemp 2008). That year was just one of many years during the sixteenth century when winters in Europe were particularly severe. Historical and physical records from many parts of the world indicate cooler temperatures for much of the period

between about 1450 and 1850 (PAGES 2k Consortium 2013). The proposed reasons for this period of cooler temperatures, often referred to as the Little Ice Age (LIA), have varied with region and include solar variability [Eddy 1976; for review see Lean (2010)], periods of strong and frequent tropical volcanic eruptions (Miller et al. 2012; Schurer et al. 2014), declining Northern Hemisphere summer insolation associated with the long cycles of the Earth's orbital parameters (Kaufman et al. 2009), and land use and land cover (LULC) changes (He et al. 2014). The LIA was preceded by a period of warmer temperatures from roughly 950 to 1250, the Medieval Climate Anomaly (MCA), although this period exhibited much more heterogeneity in the timing and regional expressions of the responses (Bradley et al. 2003; Diaz et al. 2011).

The last millennium has a rich archive of annually dated proxy records that give us a longer perspective on climate variability and change than is available for the instrumental period [see Jones et al. (2009) and PAGES 2k Consortium (2013) for reviews]. An extensive network of tree-ring records provides a measure of the year-to-year as well as longer-term variability of continental temperatures at mid- to high latitudes

AFFILIATIONS: OTTO-BLIESNER, BRADY, FASULLO, LANDRUM, STEVENSON, ROSENBLOOM, MAI, AND STRAND—Climate and Global Dynamics Division, National Center for Atmospheric Research, Boulder, Colorado; JAHN—Department of Atmospheric and Oceanic Sciences and Institute of Arctic and Alpine Research, University of Colorado, Boulder, Colorado

CORRESPONDING AUTHOR: Bette L. Otto-Bliesner, 1850 Table Mesa Dr., Boulder, CO 80305
E-mail: ottobli@ucar.edu

The abstract for this article can be found in this issue, following the table of contents.

DOI:10.1175/BAMS-D-14-00233.1

In final form 10 July 2015
©2016 American Meteorological Society

(e.g., Fritts et al. 1979; Briffa 2000; Cook et al. 2006) and continental moisture at low latitudes (e.g., Cook et al. 1999; 2010) over the last millennium, although the spatial coverage decreases at earlier times. Similarly, ice cores in Greenland and the Antarctic (e.g., Vinther et al. 2009; Graf et al. 2002), as well as Arctic lake records (e.g., Kaufman et al. 2009), contribute to the reconstruction of high-latitude regional temperature variability. At lower latitudes, analyses of stalagmites in caves exhibit monsoon-related variability (e.g., Wang et al. 2005) and coral records have been employed to assess the centennial-to-millennial variability of El Niño–Southern Oscillation (e.g., Cobb et al. 2003, 2013).

Because of its high data density, the last millennium is an excellent time period over which to quantify the relative importance of natural and anthropogenic forcings in explaining recent and more distant changes to climate. For this reason, it has caught the attention of policy makers and has been featured prominently in the Intergovernmental Panel on Climate Change (IPCC) reports. For phase 5 of the Coupled Model Intercomparison Project (CMIP5) and as a contribution to the IPCC's Fifth Assessment Report (AR5), modeling groups worldwide completed simulations for the period 850–1850 [hereafter referred to as the last millennium (LM)] with the same models and using the same resolutions as for future projections (Taylor et al. 2012), as compared to the ensemble of opportunity available for the IPCC AR4 (Jansen et al. 2007; Fernández-Donado et al. 2013). The forcing protocols were defined by the Paleoclimate Modelling Intercomparison Project (PMIP) and included several scenarios for solar and volcanic forcings to allow testing of the structural uncertainties in different reconstructions (Schmidt et al. 2011).

The CMIP5 LM simulations organized by PMIP3 allowed for the exploration of structural differences among the participating models and uncertainties in the reconstructed forcings. Nine modeling groups completed the CMIP5 LM simulations, using the same model versions and the same resolution as the CMIP5 future projection simulations, providing important contributions to the chapters on paleoclimate (Masson-Delmotte et al. 2013), evaluation of climate models (Flato et al. 2013), and detection and attribution of climate change (Bindoff et al. 2013) in the IPCC's AR5. Additional LM single-model ensembles separating out the individual forcing responses suggest that volcanic eruptions were the dominant forcing of Northern Hemisphere temperature before 1800, with smaller but detectable contributions from solar and greenhouse gas variations on some time

scales (Phipps et al. 2013; Schurer et al. 2013, 2014). This response holds true even when different volcanic forcing reconstructions were used (Andres and Peltier 2013; Schmidt et al. 2014).

Analyses of the CMIP5 LM simulations in comparison with reconstructions of regional temperature variability and North American drought further suggest that internal variability may play a large role on multidecadal and centennial time scales (Bothe et al. 2013; Coats et al. 2015). This agrees with the conclusion from an earlier large ensemble of LM simulations with the ECBilt/CLIO model that at the continental and subcontinental scales the contribution of internal climate variability to regional responses can be large (Goosse et al. 2005).

The Community Earth System Model-Last Millennium Ensemble (CESM-LME) expands on the CMIP5 and earlier LM model simulations by providing the largest ensemble of LM simulations with a single model to date. The CESM-LME uses the CMIP5 climate forcing reconstructions (Schmidt et al. 2011) and contains both “full forcing” simulations containing all LM forcings, as well as ensembles of simulations with each forcing individually (Table 1). This ensemble approach, using the most current version of the comprehensive CESM (Hurrell et al. 2013), allows the CESM-LME to provide a state-of-the-art counterpart to the previous multimodel studies described above. In the CESM-LME, the research community now has an important resource for understanding the role of internal variability in generating climate variations over the last 1,156 years. The scientific questions that motivated our project include the pressing need to evaluate the ability of models such as CESM to capture observed variability on multidecadal and longer time scales, to determine the characteristics (i.e., intensity, spatial structure, seasonality) of variability associated with the individual natural forcings versus purely internal variability, and to permit a longer-term perspective for detection and attribution studies.

EXPERIMENTAL DESIGN. The CESM-LME employs version 1.1 of CESM with the Community Atmosphere Model version 5 [CESM1(CAM5); Hurrell et al. 2013], the same model as the CESM-Large Ensemble (CESM-LE; Kay et al. 2015) except for the resolution of the atmosphere and land components. The CESM-LME uses $\sim 2^\circ$ resolution in the atmosphere and land components and $\sim 1^\circ$ resolution in the ocean and sea ice components. At this resolution, we can simulate $\sim 25 \text{ yr day}^{-1}$ on the National Center for Atmospheric Research (NCAR)–Wyoming

TABLE 1. CESM-LME simulations. Additional information about the simulations including the forcing datasets, saved variables, diagnostics, model support and known issues can be found at the CESM-LME website (www2.cesm.ucar.edu/models/experiments/LME).

Expt	No. of runs	Solar variability	Volcanic eruptions	Land use	GHGs	Orbital changes	Ozone-aerosols
Full forcings	10	Transient 850–2005	Transient 850–2005	Transient 850–2005	Transient 850–2005	Transient 850–2005	Transient 1850–2005
Solar only	4	Transient 850–2005	None	*	*	*	1850
Volcanic only	5	*	Transient 850–2005	*	*	*	1850
Land use only	3	*	None	Transient 850–2005	*	*	1850
GHG only	3	*	None	*	Transient 850–2005	*	1850
Orbital only	3	*	None	*	*	Transient 850–2005	1850
Ozone-aerosol only	2	*	None	*	*	*	Transient 1850–2005

* Fixed at 850 values.

Supercomputing Center (NWS) Yellowstone computer, and complete a full simulation from 850 to 2005 in ~45–50 days.

Before starting the CESM-LME simulations, we spun up the model for an 1850 control simulation of 650 yr, from which an 850 control simulation was branched and run for an additional 1,356 yr (Fig. 1). All CESM-LME simulations were started from year 850 of the 850 control simulation (i.e., after 200 yr of the 850 control). The only difference among ensemble members is in the application of small random roundoff (order 10^{-14} °C) differences in the air temperature field at the start of each ensemble member. Both control simulations were run in excess of 1000 yr to overlap with the CESM-LME simulations, allowing removal in our analyses of any trends still present. In surface temperature and top-of-atmosphere (TOA) net incoming flux, these trends are on the order of $0.02^{\circ}\text{C century}^{-1}$ and 0.01 W m^{-2} , respectively. For sea ice area, there is no significant trend in the control simulation. Over the period from 850 to 1849, the global mean ocean temperature in the 850 control integration cools by only $\sim 0.004^{\circ}\text{C century}^{-1}$, reflecting a continuing adjustment toward equilibrium in the deepest ocean levels

below ~500 m. The global mean ocean salinity freshens by $\sim 5 \times 10^{-5} \text{ psu century}^{-1}$, indicating an insignificant adjustment between global freshwater reservoirs.

The choices of LM forcings and their implementations follow those used in our LM simulation with the Community Climate System Model, version 4 [CCSM4; see Landrum et al. (2013), in particular Fig. 1 and its discussion for more details]. The forcings over this period include orbital, solar, volcanic, changes in land use/land cover, and greenhouse gas levels. We adopt the concentrations of the well-mixed greenhouse gases (CO_2 , CH_4 , and N_2O) from high-resolution Antarctic ice cores (Schmidt et al. 2011) and calculate the seasonal and latitudinal distribution

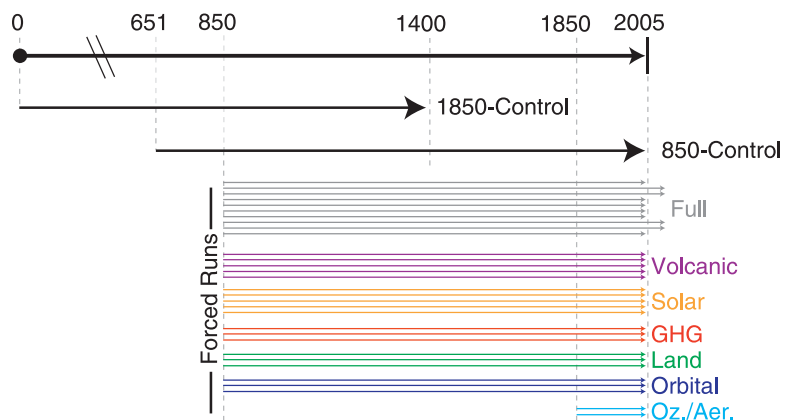


FIG. 1. Details of the initial states and simulation lengths of the CESM-LME control and forced runs.

of the orbital modulation of insolation from the equations in Berger (1978). For the volcanic forcing, we adopt version 1 of the Gao et al. (2008) ice-core-derived estimates of aerosol loadings as a function of latitude, altitude, and month. Stratospheric aerosols are prescribed in the CESM as a fixed single-size distribution in the three layers in the lower stratosphere above the tropopause. Changes in total solar irradiance (TSI) are prescribed using the Vieira et al. (2011) reconstruction, upon which an estimated 11-yr solar cycle has been imposed and spectral solar irradiance is derived using linear regression of TSI at each spectral interval [see Schmidt et al. (2011) for details]. We merged the Pongratz et al. (2008) reconstruction of land use with that of Hurtt et al. (2011), scaling the Pongratz dataset to match the Hurtt dataset at 1500 at every land model grid. This procedure resulted in a very small step change in land cover at 1500, which is not important from a physical climate perspective but is potentially important for some applications (Lehner et al. 2015). The only plant functional types (PFTs) that are changed are those for crops and pasture; all other PFTs remain at their 1850 control prescriptions.

For the continuation of the CESM-LME simulations from 1850 to 2005, we adopted the same forcings as the CESM-LE with the exception of including orbital changes in insolation not considered in the CESM-LE. The CESM-LME-adopted ozone and aerosol forcings are fixed at the 1850 control values until 1850 and then include the evolving anthropogenic changes to 2005.

The CESM-LME forcings are detailed in Fig. 2. Volcanic events of varying strength have been a recurring feature of the last millennium (Fig. 2a), with periods of frequent, large tropical eruptions in the last half of the thirteenth century and the first half of the nineteenth century. The largest eruptions in terms of estimated total global stratospheric volcanic sulfate aerosol injection occurred in 1258 (Samalas in Indonesia; 257.9 Tg), 1452 (Kuwae of Vanuatu; 137.5 Tg), and 1815 (Tambora in Indonesia; 109.7 Tg). For context, the 1991 Mount Pinatubo eruption had a total global stratospheric volcanic sulfate aerosol injection estimated at 30.1 Tg (Gao et al. 2008). It should be noted that there are major differences in both the timing and magnitude of the volcanic forcings between the two suggested PMIP3 reconstructions (Gao et al. 2008; Crowley and Unterman 2013), as shown in Schmidt et al. (2011), arising from different methodologies and uncertainties inherent in reconstructing volcanic deposition events from polar ice cores. Solar variability is characterized by a pronounced quasi-11-yr sunspot cycle in insolation

of about 1 W m^{-2} , a variability that itself changes with time. Sunspot counts back to 1610 and longer, indirect records of solar activity from ice cores and tree rings also indicate periods of ~ 70 – 100 yr with reduced solar activity. These include the Wolf (~ 1280 – 1350), Sporer (~ 1460 – 1550), and Maunder (~ 1645 – 1715) grand solar minima, with an increase in the TSI of about 0.1% from the Maunder Minimum to today (Fig. 2b). Concentrations of major greenhouse gases were largely stable prior to the late nineteenth century, with only relatively small variations related to natural feedbacks in the carbon and nitrogen cycles. Major increases in CO_2 , N_2O , CH_4 , and $\text{F}_{11/12}$ occurred during the twentieth century (Fig. 2c). Over the past two centuries, there has also been a substantial increase in crop and pasture extent, amounting now to nearly a third of all land regions (Fig. 2d). When the magnitudes of these forcings are estimated from the net TOA tropical clear-sky shortwave flux over ocean (Fig. 2e), a region chosen to minimize the influence of land and the cryosphere, the decadal-mean variability associated with volcanic events (several W m^{-2}) dominates that of other sources (orbital and LULC contributions not shown for clarity and as a result of their small net forcing over tropical oceans). Solar variability acts as a secondary source of variability ($\sim 0.2 \text{ W m}^{-2}$), an influence that, for example, is weak but evident from 1650 to 1750 (Fig. 2e).

We have completed 30 CESM1(CAM5) simulations for the CESM-LME project. These include an ensemble of 10 simulations with all forcings as well as smaller ensembles with each forcing separately (Table 1, Fig. 1). To assess the influence of anthropogenic-forced changes in ozone and aerosols, we completed two simulations starting with the year 1850 of the control simulation and continuing to 2005. One full-forcing ensemble member (7) saved 6-hourly atmospheric output for forcing regional models and extremes analyses, and one full-forcing ensemble member (10) included the simulation of radiocarbon in the ocean for comparison to related proxies. We also extended four full-forcing ensemble members to 2100 with the highest representative concentration pathway (RCP8.5) forcing and completed the CMIP6 abrupt $4 \times \text{CO}_2$ and 1% to $4 \times \text{CO}_2$ experiments.

RESULTS. In this section, we illustrate some examples of the capabilities and applications of the CESM-LME. We compare to proxy reconstructions, where possible, to provide an important first benchmark for validating the CESM-LME.

Surface temperature. Northern Hemisphere (NH) mean surface temperature has been estimated from

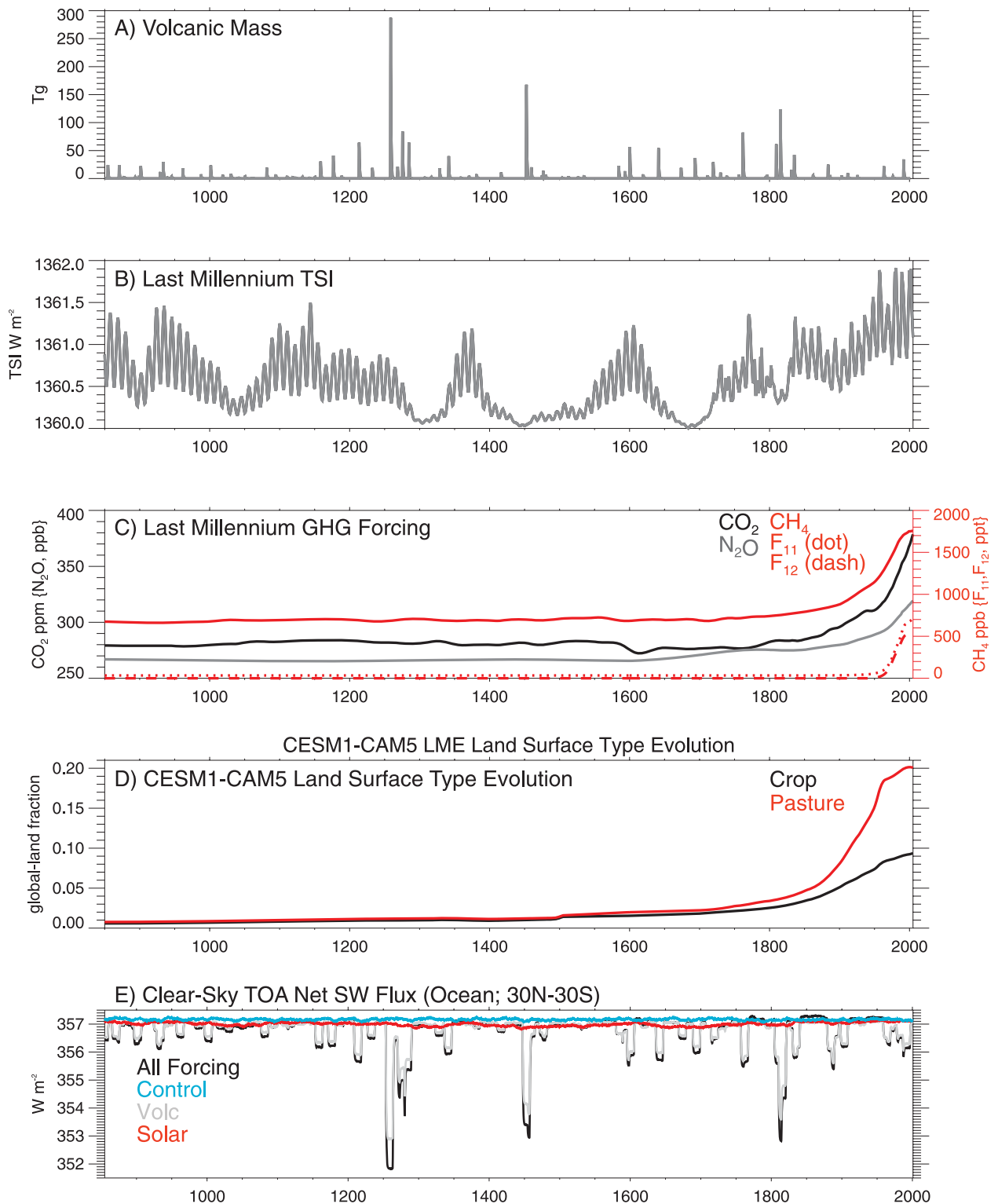


FIG. 2. Evolution of the major forcings used for the CESM-LME including (a) volcanic mass, (b) TSI, (c) GHG concentrations, (d) crop and pasture extent, and (e) TOA net clear-sky shortwave flux over the tropical oceans.

numerous proxy reconstructions (Mann et al. 2009; Ammann and Wahl 2007; Moberg et al. 2005; Juckes et al. 2007). Here, we compare the ensemble mean of

CESM-LME full-forcing runs to five reconstructions for the NH surface temperature (Fig. 3) included in the AR5 [see Masson-Delmotte et al. (2013)

for discussion of the reconstruction methods and uncertainties]. The simulated NH surface temperature confirms the reconstructed “hockey stick”-like pattern with generally warm conditions near 1100 (coincident with the Medieval maximum of TSI and only weak volcanic activity) and a gradual cooling until the nineteenth century. The CESM-LME resolves cooling events associated with major volcanic eruptions (1258, 1452, and 1815), and sustained intervals of cool temperatures during the late thirteenth century, from the early seventeenth to the mideighteenth centuries, as well as during the early nineteenth century. The degree of volcanic cooling in the CESM-LME is generally stronger than in the reconstructions, possibly related to uncertainties in the volcanic forcing (Sigl et al. 2014).

The most notable feature of both the simulated and reconstructed records is the large warming evident since the late nineteenth century, the timing and magnitude of which differ across reconstructions but whose overall magnitude is well observed in the instrumental period. The CESM-LME simulations capture about 80% of the observed twentieth-century warming; this underestimate is likely due to overly strong indirect aerosol forcing. CESM1 is known to

simulate a stronger aerosol indirect effect than did CCSM4, which overestimated the heat gain since 1970 (Gent et al. 2011; Meehl et al. 2012); CESM thus performs comparably to CCSM4, but errs on the side of overly strong twentieth-century cooling associated with aerosols. The observed trend from the Goddard Institute for Space Studies (GISS) Surface Temperature Analysis (GISTEMP) over 1930–2005 is $0.68^{\circ}\text{C century}^{-1}$ while in the ensemble means for the CESM-LE and CESM-LME simulations they are 0.56°C and $0.54^{\circ}\text{C century}^{-1}$, respectively.

The CESM-LME full-forcing simulations are able to capture the overall globally warmer conditions during the MCA (950–1250) relative to the LIA (1450–1850) present in the proxy record; global average annual temperature differences range from 0.12° to 0.17°C and NH annual temperature differences from 0.16° to 0.21°C (Figs. 4 and 5). As shown in Fig. 2, the most significant differences in radiative forcing between the MCA and LIA are the very large volcanic eruptions during the LIA as compared to only weak volcanic activity during the MCA. The simulated response shows polar amplification of the simulated temperature responses, particularly in the Arctic ($\sim 3\text{--}4$ times the global temperature

change), more muted temperature changes in the tropics, and greater temperature changes over the continents than the oceans. The order of magnitude of warming regions in the CESM-LME full-forcing simulations is similar to the annual temperature reconstruction of Mann et al. (2009). The polar regions, where the simulations indicate the largest temperature anomalies between the MCA and LIA, are not reported in the reconstruction because of the challenges involved in validating proxy records.

As compared to the CMIP5 LM simulations, the CESM-LME simulations simulate larger MCA-LIA NH surface temperatures differences than $2/3$ of these models (Fig. 5). Notably, the mean of the

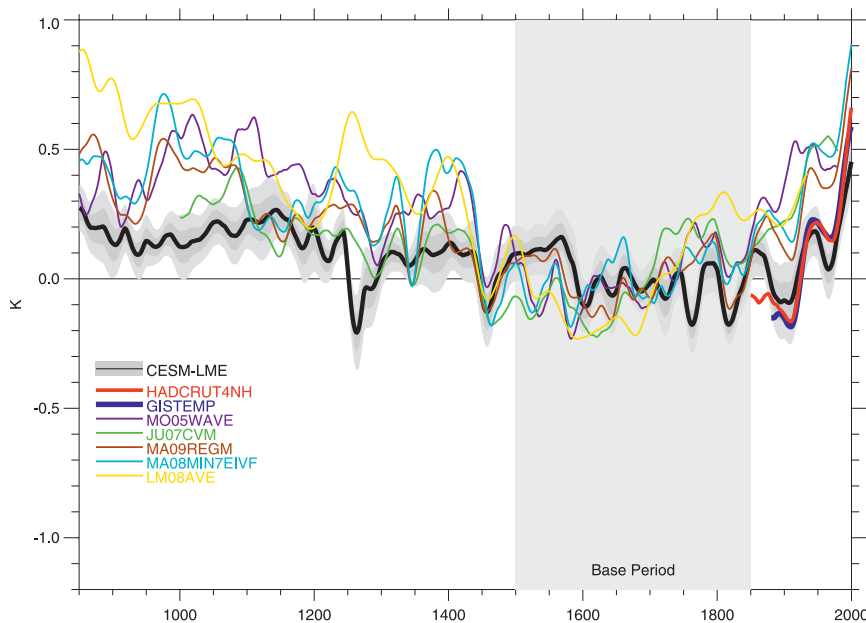


FIG. 3. NH annual surface temperature anomalies (K) for the mean of the full-forcing runs (black) with 1σ (dark gray) and 2σ (light gray) ranges vs various reconstructions and instrumental observations: Hadley Centre/Climatic Research Unit, version 4 (HADCRUT4NH; Morice et al. 2012), and GISTEMP (Hansen et al. 2010). As in the AR5, anomalies are computed relative to the base period of 1500–1850. A 20-yr Gaussian smoothing has been applied. Reconstructions plotted are MO05WAVE (Moberg et al. 2005), JU07CVM (Juckes et al. 2007), MA09REGM (Mann et al. 2009), MA08MIN7EIVF (Mann et al. 2008), and LM08AVE (Loehle and McCulloch 2008).

full-forcing CESM-LME simulations (0.19°C) is less than the warming of the CCSM4 simulation, as are the values for all individual ensemble members. The single-forcing ensemble members indicate that the volcanic forcing is most important for explaining the MCA-LIA NH surface temperature differences, with a three-member mean of 0.11°C . Interestingly, in CESM(CAM5) the LULC changes from MCA to LIA make the next most important contribution to the NH surface temperatures changes. Over half of the PMIP3 models did not use land-use/cover changes as an LM forcing, indicating that this could contribute to some of the underestimates of MCA-LIA temperature differences in CMIP5 LM simulations.

The most striking first impression is that the ensemble members are quite similar with notable differences only coming into sight by zooming in. Strong reconstructed surface temperature differences between the MCA and LIA over northern Europe are simulated in some, but not all, ensemble members (Fig. 4). This is consistent with previous CCSM3 modeling studies that indicate cooling over northern Europe and the North Atlantic associated with the negative radiative forcing of large volcanic eruptions during the LIA (Zhong et al. 2011; Lehner et al. 2013), with the relative response sensitive to the initial state of the ocean and atmosphere during the eruptions (Zhong et al. 2011).

The importance of internal variability is also illustrated when comparing the CESM-LME full-forcing

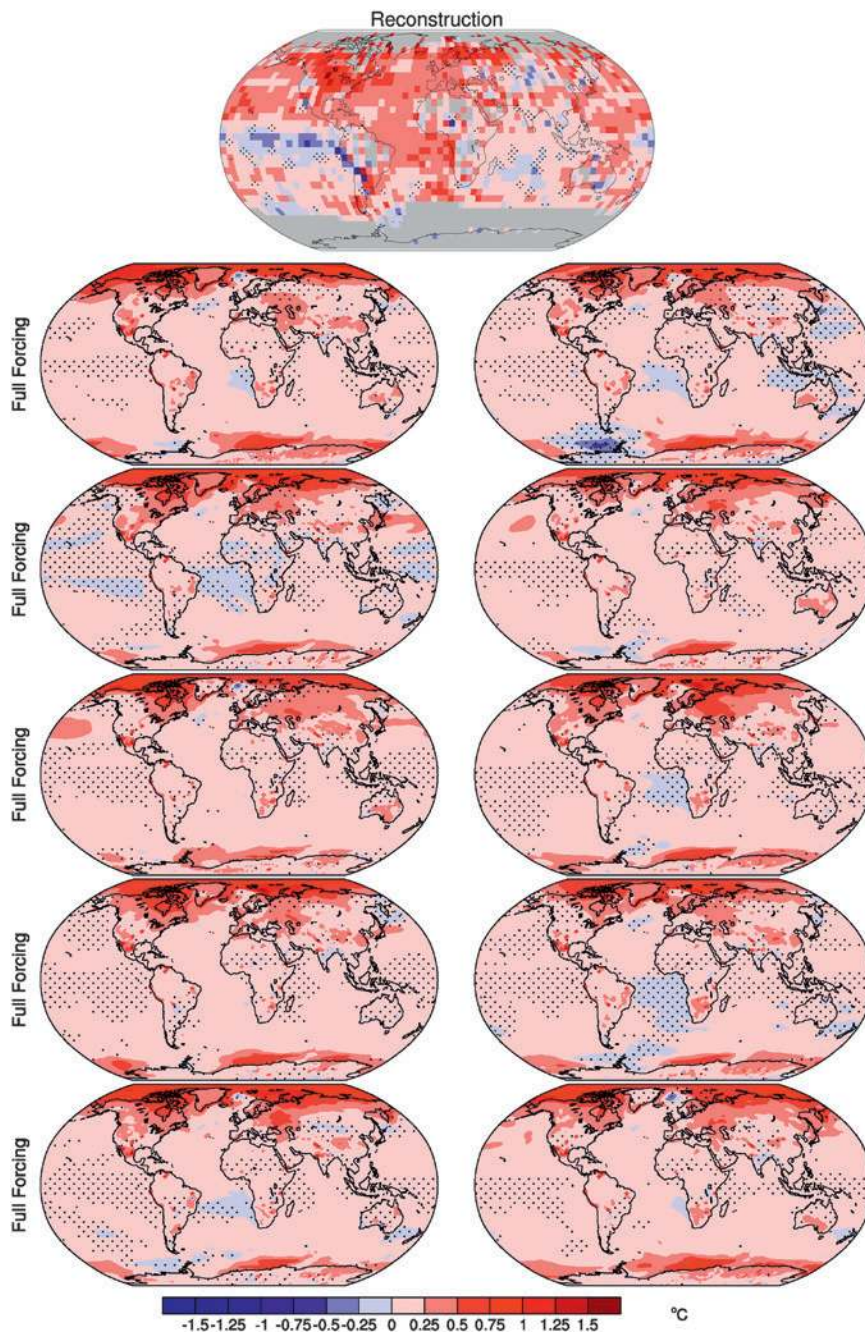


FIG. 4. Annual surface temperature changes ($^{\circ}\text{C}$), MCA (950–1250) minus LIA (1450–1850), from Mann et al. (2009) proxy-based reconstruction are shown in the top panel and in the remaining panels the changes as simulated in the 10 CESM-LME full-forcing simulations. Stippling indicates differences not statistically significant at the 95% level using a Student's *t* test.

simulations to the CMIP5 LM simulations for June–August land surface temperatures for Europe (Fig. 6). The CESM-LME ensemble spread suggests that at least a portion of the CMIP5 LM multimodel spread of summer surface temperatures over Europe may be attributable to internal variability. Differences in both the timing and magnitude of the volcanic forcing

between the two suggested PMIP3 reconstructions are visible in the summer temperature responses over Europe. The Hadley Centre Coupled Model, version 3 (HadCM3), and Max Planck Institute Earth System Model, paleoclimate (MPI-ESM-P), LM simulations use the Crowley and Unterman

(2013) volcanic reconstruction. Notably, this volcanic reconstruction concluded that the aerosols from the 1783 Laki eruption in Iceland remained mostly in the troposphere. The late thirteenth-century pulse of eruptions also has notable differences between the two reconstructions.

Over North America, all the CESM-LME full-forcing simulations exhibit warmer conditions during the MCA than the LIA, although they underestimate the magnitude of the surface temperature differences as compared to the Mann reconstruction (Figs. 4 and 7). The much higher surface temperatures during the MCA as compared to the LIA are only robust regionally across the full-forcing ensemble for Hudson Bay and the Canadian Arctic Archipelago. Each of the individual LM forcings contributes to this pattern of a warmer MCA than LIA in the Canadian Arctic, but only the volcanic-only and orbital-only simulations consistently so (though not always above the 95% confidence criteria). For solar-only forcing and greenhouse gas (GHG)-only forcing, not all ensemble members reproduce the pattern of warming in the Canadian Arctic, illustrating the utility of ensembles of simulations for attribution of Arctic climate responses. Interestingly, at least in some regions the role of single forcing agents can be discriminated: the warming in the southwestern United States and Mexico is caused by land-use changes in CESM.

In our simulations, the late twentieth-century global-mean warming cannot be solely explained by increased solar irradiance during the twentieth century (Scafetta and West 2008). Figure 8 shows annual surface temperature anomalies, for the present day (PD; 1950–2000) minus LIA (1450–1850), for the

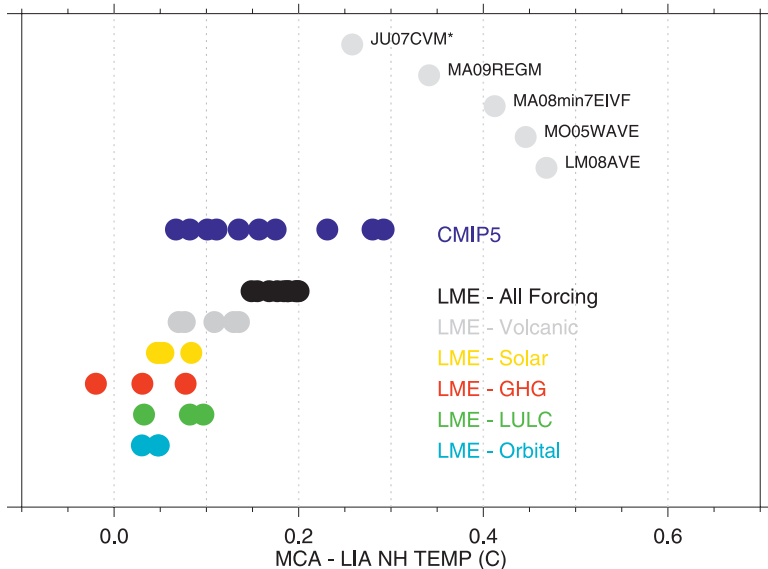


Fig. 5. NH annual surface temperature changes (°C), MCA (950–1250) minus LIA (1450–1850), for reconstructions plotted in Fig. 3, CMIP5 LM simulations, and each of the CESM-LME ensemble members.

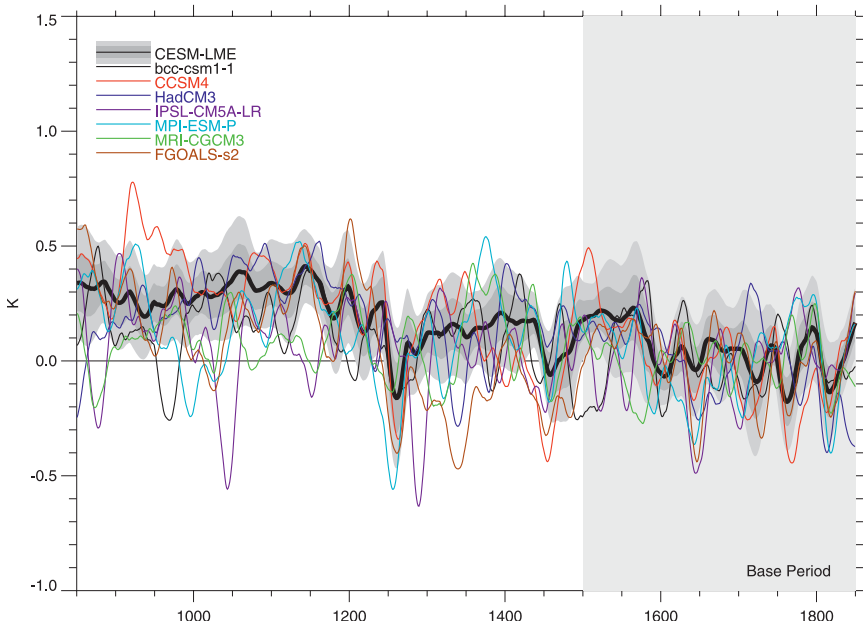


Fig. 6. Jun–Aug land surface temperature anomalies (°C) for Europe (35°–70°N, 5°W–40°E) for the mean of the full-forcing runs (black) with 1σ (dark gray) and 2σ (light gray) ranges vs the CMIP5 LM simulations. Anomalies are computed relative to the base period of 1500–1850. A 20-yr Gaussian smoothing has been applied.

MCA (950-1250) - LIA(1450-1850)

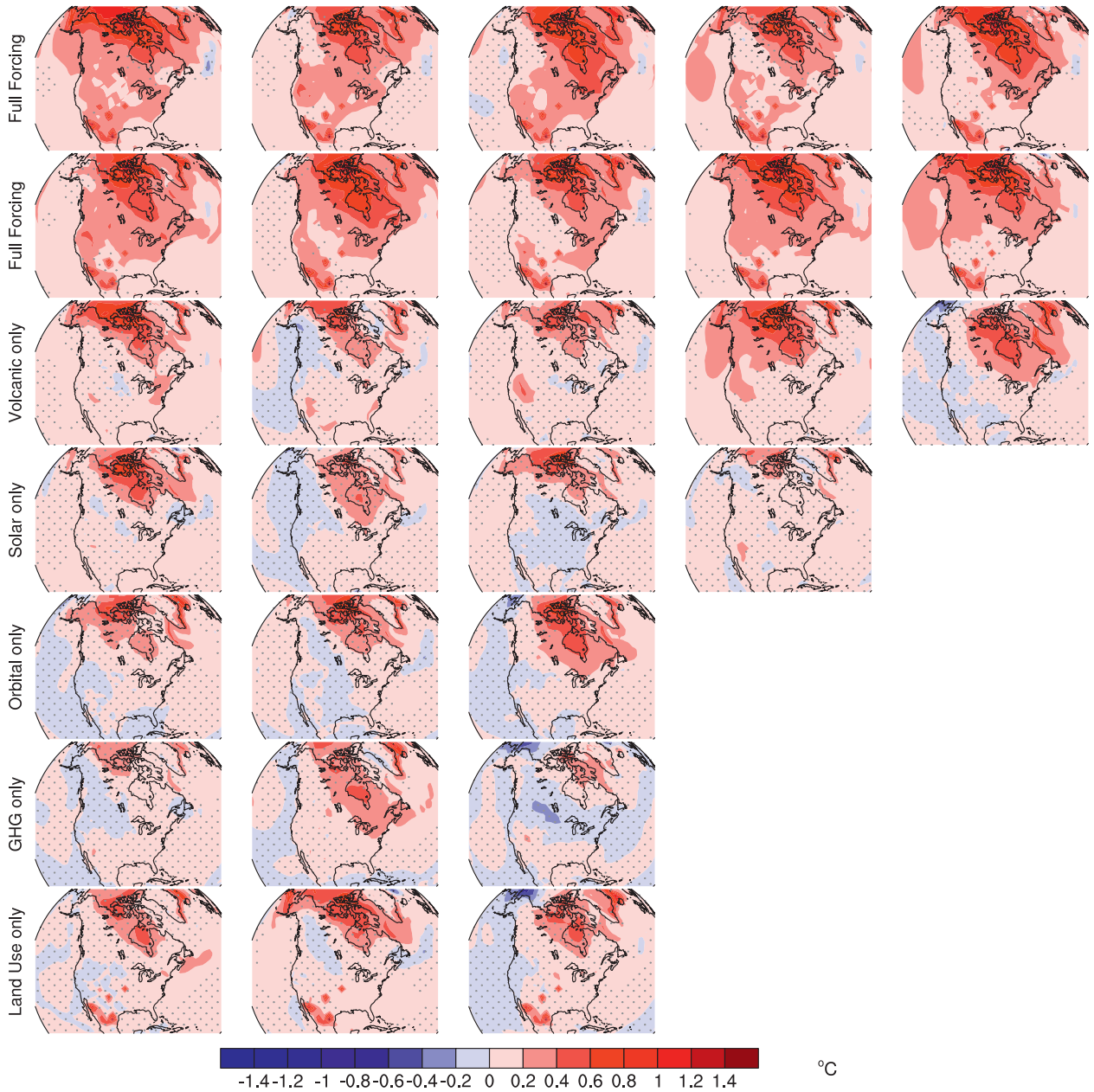


FIG. 7. Annual surface temperature changes (°C), MCA minus LIA, over North America, as simulated in the CESM-LME full- and single-forcing simulations. Stippling indicates differences not statistically significant at the 95% level using a Student's t test. See Fig. 4 for definitions of time periods.

single-forcing and full-forcing CESM-LME runs. For each forcing scenario, ensemble members with minimum and maximum global temperature differences are shown. The increased GHG at the end of the twentieth century result in strong simulated warming over the entire globe, with the exception of the North Atlantic region. The simulated small cooling in the latter region is associated with a weakening of the simulated Atlantic meridional

overturning circulation (AMOC) in the twentieth century. Cooling due to strongly increased Northern Hemisphere aerosols during the twentieth century counteracts approximately half of the simulated GHG warming in the Northern Hemisphere. The twentieth-century aerosol loadings in the Southern Hemisphere are smaller and as such the simulated cooling associated with the aerosols is much less than in the Northern Hemisphere. Sea ice plays an

important feedback in the model responses to the GHG and aerosol increases during the twentieth century (see *Sea ice* section below). Increases in solar irradiance from the Maunder Minimum to the late twentieth century (~0.1% in our reconstruction) force a more modest, consistent warming over the Arctic Ocean and North America. The other forcings—volcanic, orbital, and land use—have much less effect on the surface temperature changes simulated for the last half of the twentieth century as compared to the LIA.

Sea ice. Arctic sea ice has been declining rapidly over recent decades (e.g., Stroeve et al. 2008), with large contributions from both forced anthropogenic trends and internal variability (Swart et al. 2015). Prior to the second part of the twentieth century, Arctic sea ice records are sparse, but the existing reconstructions suggest that the recent Arctic sea ice loss has been unprecedented during the last 1,400 years (e.g., Kinnard et al. 2011). By looking at the different CESM-LME single-forcing simulations compared to the 10-member full-forcing CESM-LME,

we can begin to attribute features in the full-forcing simulation to individual forcings over the last millennium, allowing us to put the recent changes into a longer-term context.

In agreement with the sea ice reconstructions for the last millennium by Kinnard et al. (2011), the largest signal in the sea ice extent in the CESM-LME simulations is the strong decline in the NH sea ice extent over recent decades (Fig. 9). By looking at the single-forcing simulations, it is clear that this decline is driven by GHG. In the NH, the sea ice decline in the GHG-only simulations already starts in 1850, but other forcings, in particular the ozone–aerosol forcing and the volcanic forcing, delay and reduce the magnitude of the realized sea ice extent decline in the fully forced simulations. In the SH, the effect of the GHG forcing on sea ice is offset less than in the NH, resulting in a very strong decline of the sea ice extent in the SH since 1850. Over the last three decades for which satellite data are available, this simulated strong decline in SH sea ice extent conflicts with satellite data that shows a small positive trend in SH sea ice extent (e.g., Cavalieri and Parkinson 2012). This

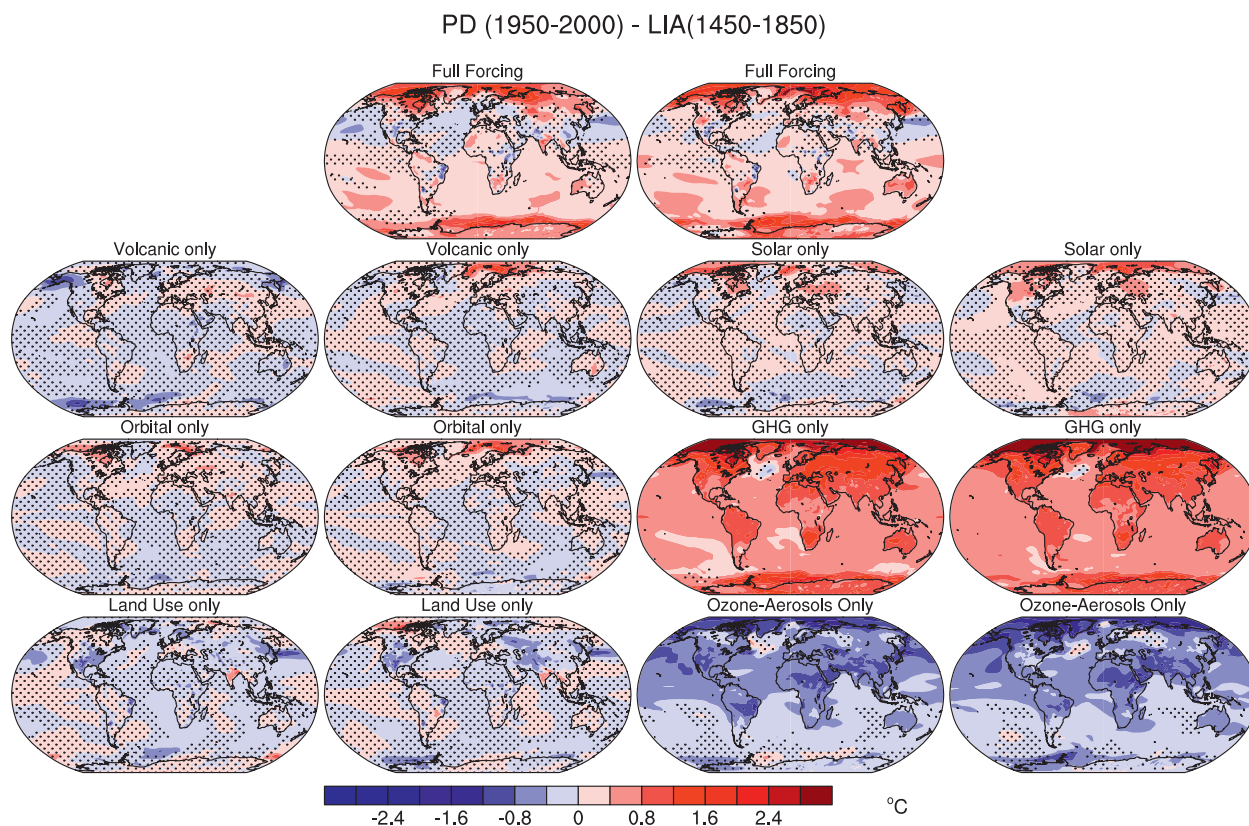


FIG. 8. Annual surface temperature anomalies (°C), PD (1950–2000) minus LIA (1450–1850), as simulated in CESM-LME. Shown for each forcing set are the ensemble members with (left) minimum and (right) maximum global average temperature differences. Stippling indicates differences not statistically significant at the 95% level using a Student’s *t* test.

mismatch with the data represents a common feature of many climate model simulations (e.g., Turner et al. 2013) and the causes are still under investigation.

Prior to the sea ice decline due to GHG, sea ice extent had been slowly increasing in both hemispheres (Fig. 9), in agreement with the slow cooling over that period (Fig. 3) and with sea ice reconstructions for the NH (e.g., Massé et al. 2008). Superimposed on the slowly increasing sea ice prior to 1850, some strong volcanic forcing events are clearly visible in the fully forced ensemble mean (e.g., for the NH around 1825 and 1260). Furthermore, it is clear from the fully forced ensemble spread that significant internal variability has occurred over the last millennium, making it important to employ ensembles to investigate the detailed climatic impact of, and driving forces behind, sea ice changes.

Precipitation and drought. Anthropogenic forcing is expected to lead to large changes in twenty-first-century hydroclimate, with most models projecting drying trends over North America (Wuebbles et al. 2014; Cook et al. 2015). Additionally, proxy records indicate that decadal-to-multidecadal “megadroughts” are quite common in many locations

(Woodhouse and Overpeck 1998); using the CESM-LME, we can gain insight into the drivers of such events and the degree to which anthropogenic effects may dominate.

To illustrate the twentieth-century trends in the CESM-LME, Fig. 10 shows the differences in the Palmer drought severity index (PDSI) between 1950 to 2000 and 850 to 1850, as well as the same quantities calculated using the *North American Drought Atlas (NADA)* tree-ring reconstruction (Cook et al. 2004). The CESM-LME full-forcing ensemble (Fig. 10a) shows overall drier conditions in the western United States and northern Mexico during the late twentieth century, with wetting in the Midwest and the eastern United States. Single-forcing runs suggest that the drying trend in the western United States is due primarily to greenhouse gases, while the wetting in the east is dominated by land-use/land-cover changes (Figs. 10c,e). Other forcings contribute only a minor amount. Agreement with the *NADA* is quite good over Mexico and the eastern United States, but the *NADA* does not show the drying trend over the western United States; this may reflect contributions from internal variability (cf. Figs. 10a and 10b).

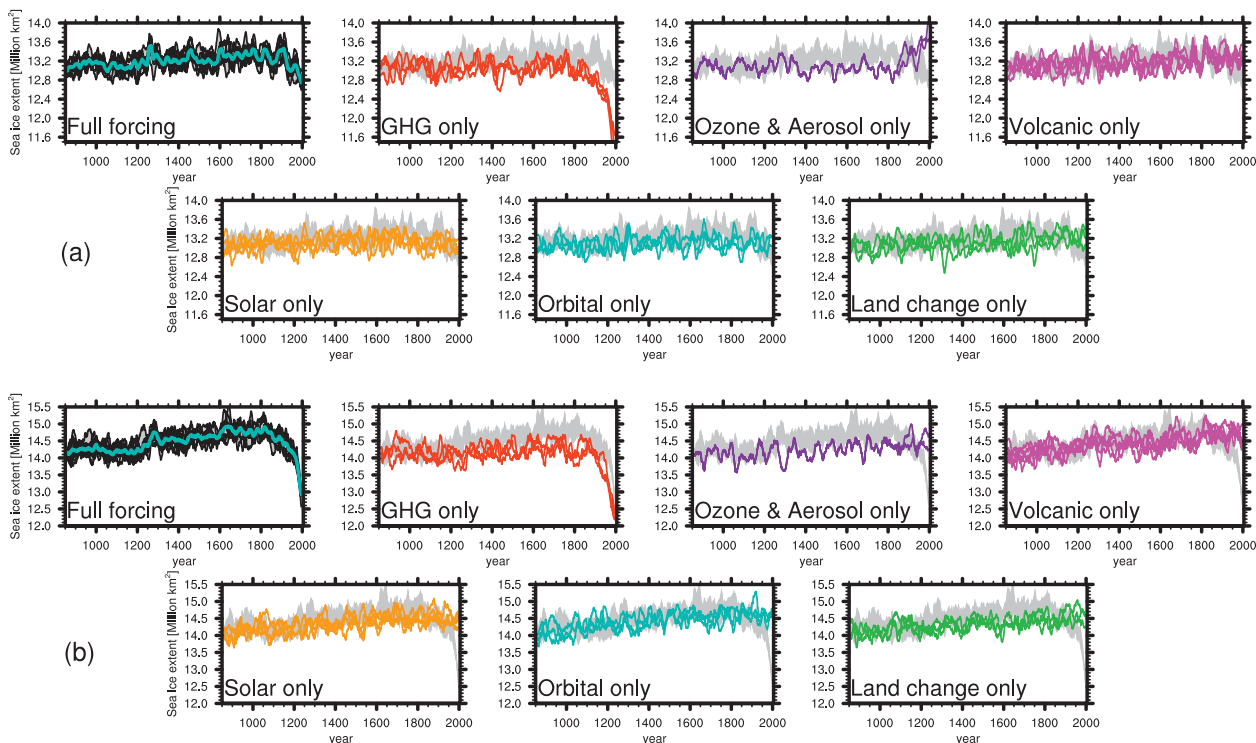


FIG. 9. Annual mean sea ice extent (million km²) for the (a) Northern and (b) Southern Hemispheres in the CESM-LME single-forcing and the full-forcing ensemble simulations (smoothed with a 20-yr running mean). The ensemble spread in the full-forcing ensemble is shown by gray shading in all panels and the ensemble mean of the 10 fully forced ensemble members is shown in cyan in the full-forcing panels.

Climate variability. Modes of internal climate variability affect regional patterns of temperature and precipitation. The influence of forcings on both global mean and lateral gradients in radiative fluxes provides a means by which they may interact with

these modes. While various reconstructions have suggested multidecadal-to-centennial modulation of these modes by past forcings (e.g., Trouet et al. 2009; Li et al. 2011; Knudsen et al. 2011), the extent to which natural forcings over the past millennium have acted as a pacemaker for these modes remains an open but important question for constraining near-term future projections and improving risk estimates.

The spectra of two key modes of variability are shown in Fig. 11, where the CESM-LME simulations are differentiated into groups that do not incorporate volcanic forcing, that include volcanic forcing, and that incorporate all forcings, along with their associated 1σ range. A role for volcanic forcing in increasing the power of the Atlantic multidecadal oscillation [AMO, defined as the area-weighted North Atlantic SST anomalies from 0° to 60°N and from 80°W to 0° after removing the global (60°S to 60°N) SST anomalies] at low frequency is suggested as the ensemble mean power of both the all-forcing and volcanic-forcing runs lies consistently above the range of power in the distribution of runs without volcanic forcing. Differences in the power exhibited by the Niño-3.4 index (defined as the area-weighted monthly SST from 5°S to 5°N and from 120° to 170°W after removing the long-term monthly means) are also considerable at various bands; however, the spread among the ensemble members is also considerable, and at no frequency is the distribution of either the all-forcing or volcanic-forced runs outside of the spread of spectra evident in the control simulation and CESM-LME runs without volcanic forcing.

Previous model simulations indicate a positive correlation of the AMO with the AMOC, although the lead-lag relationship varies

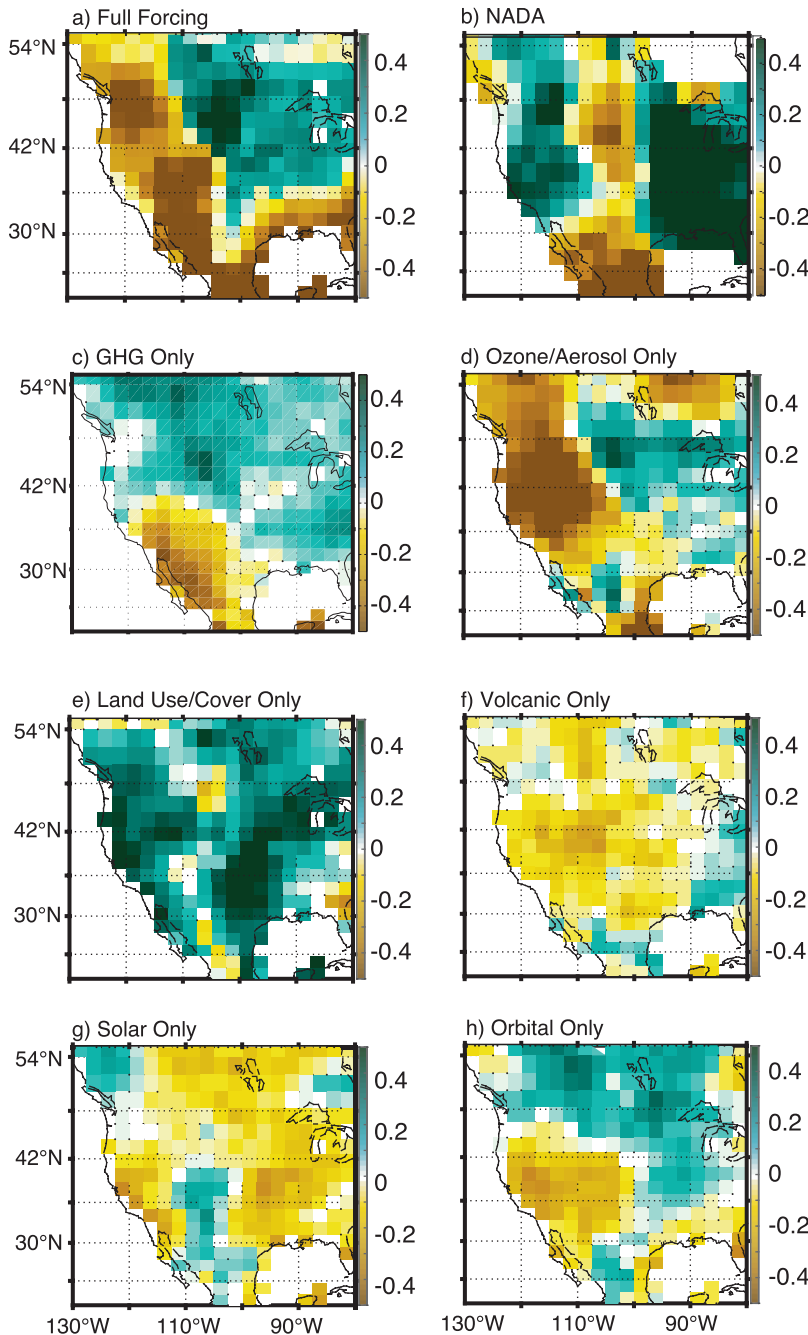


FIG. 10. PDSI composite differences between 1950–2000 and 850–1850 in (a), (c)–(h) CESM-LME and (b) the observations (NADA; Cook et al. (2004)). Model PDSI is computed using the Penman–Monteith potential evapotranspiration method; negative values indicate drier conditions for 1950–2000 relative to 850–1850, and positive values indicate wetter conditions. Stippled locations show no significant difference between the 1950–2000 and 850–1850 periods, using a two-tailed t test.

with model and forcing (Delworth and Mann 2000; Ottera et al. 2010). The CESM-LME AMOC, NH annual mean sea ice extent (SIE), and AMO all show significant responses to the seven largest volcanoes for 30, 12, and 20 yr after an event, respectively (Fig. 12). The composite response shows that the AMO cools immediately, whereas sea ice increases markedly for 2 yr and then decreases continuously for another ~10 yr. AMOC strength increases, and the increase of the AMO 2 yr postevent is consistent with significant correlations with the AMOC (Danabasoglu et al. 2012). The AMOC strengthens for ~14 yr after an event, then gradually decreases to

preevent levels 30 yr postevent. We also found that while both NH SIE and the AMO respond similarly to medium-sized volcanic eruptions (–4 to –10 W m^{–2} reduction in solar flux), the AMOC does not.

El Niño–Southern Oscillation (ENSO) accounts for the majority of interannual climate variations and is expected to respond to external forcing through a variety of feedback processes (Collins et al. 2010). The available proxy data suggest a possible increase in ENSO variance over the last millennium (e.g., Cobb et al. 2013; McGregor et al. 2010; see Fig. 13c), although the magnitude of the reconstructed increase is fairly modest. In the CESM-LME, ENSO has a realistic spread in the frequency domain although its amplitude is overestimated compared with observations; this problem is present in the higher-resolution CESM-LE simulations as well, to a somewhat lesser extent (Kay et al. 2015).

Figure 13a shows the running variance of the Niño-3.4 index in the CESM-LME: consistent with the lack of response in the overall Niño-3.4 power spectrum in Fig. 11, little systematic change is seen during epochs of varying solar irradiance and the running variance does not respond to volcanic eruptions. Some CESM-LME simulations do show a trend toward higher Niño-3.4 variance during the twentieth century, but the ensemble-mean change in variance does not exceed the bounds of internal variability until the very end of the simulation. Additionally, trends in variance are

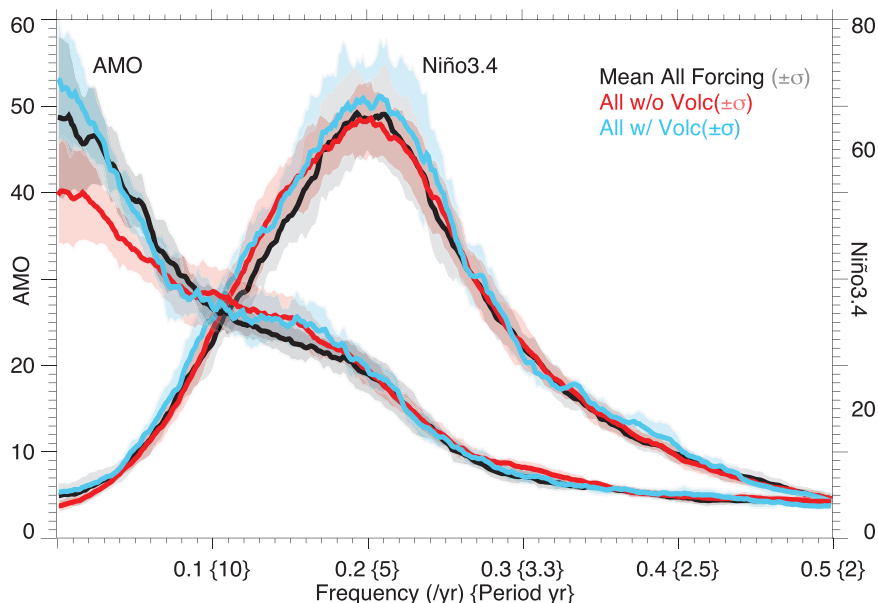


FIG. 11. Ensemble-mean AMO and Niño-3.4 power spectra [$^{\circ}\text{C}^2 (\text{cycles yr}^{-1})^{-1}$] and the associated standard deviation range for full-forcing runs (black), all runs without volcanic forcing (red), and runs with volcanic aerosols (blue). The time period used is 850–1849, and thus excludes the ozone–aerosol forcing runs. The 850 control run is included in the “without volcanic forcing” set.

not consistent among all realizations of the 850–2005 period. Figures 13b and 13c show, respectively, a stacked coral $\delta^{18}\text{O}$ record from the tropical Pacific (Cobb et al. 2013) and the CESM-LME Niño-3.4 running variance restricted to only periods during which coral data exist; the trends estimated from such gap-filled records differ in magnitude as well as sign, suggesting that both internal variability and data availability limit our ability to estimate anthropogenic influences on ENSO strength. We note also that twentieth-century trends in ensemble-mean Niño-3.4 variance differ between the CESM-LME and CESM-LE simulations (not shown), perhaps as a result of changes to the strength of the ENSO-relevant feedbacks.

The Mount Tambora eruption of April 1815, one of the largest eruptions during the historical period, caused both local devastation and widespread human and climate impacts for several years following. The subsequent year became known as “the year without a summer” because of the unusually cold and wet summer conditions in North America and Europe (Stommel and Stommel 1983; Stothers 1984) that led to poor harvests and famine. It is the third-largest eruption in terms of stratospheric aerosol forcing since 850, yielding an anomalous reduction in TOA clear-sky solar flux over the tropical ocean of more than –4 W m^{–2} in the decadal mean (Fig. 2e) and a peak monthly reduction in excess of –27 W m^{–2}.

Past studies using historical observations and proxy data have argued that large tropical volcanic eruptions lead to an El Niño-like warming in the posteruption period (Handler 1984; Adams et al. 2003; McGregor et al. 2010; Wahl et al. 2014), but these results remain controversial (Self et al. 1997;

Robock 2000). Figure 14 illustrates the benefit of using an ensemble approach to study the relationship between ENSO and large tropical eruptions. Individual realizations of the cold season tropical Pacific sea surface temperature anomalies 1 yr after the Tambora eruption peaks are shown in Fig. 14 as well as the ensemble mean

of the 15 ensemble members with volcanic forcing. The ensemble mean, as well as nine of the individual realizations, exhibit an El Niño-like warming in the eastern Pacific. This is significantly greater than the average likelihood for an El Niño to occur in any given cold season. The other six ensemble members simulate cooler temperatures or no change in the cold season tropical surface temperature anomalies 1 yr after the Tambora eruption.

SUMMARY, NEXT STEPS, AND COMMUNITY INVOLVEMENT. The CESM-LME provides a more comprehensive look at climate variability since 850 CE than has been previously available to the community. Our initial analyses of the CESM-LME highlight the importance of an ensemble approach to investigating the detailed climate responses chronicled by the proxies. That said, the present ensemble does not completely account for uncertainties in the magnitudes of forcing factors; we chose one of the possible reconstructions for each of the forcings of the LM (Schmidt et al. 2011) for our simulations. Alternate reconstructions have since become available. For land use, the reconstruction of Kaplan et al. (2011) estimates the total global land-use/land-cover change at 1850 to be approximately twice as large as that in the Hurtt et al. (2011) or

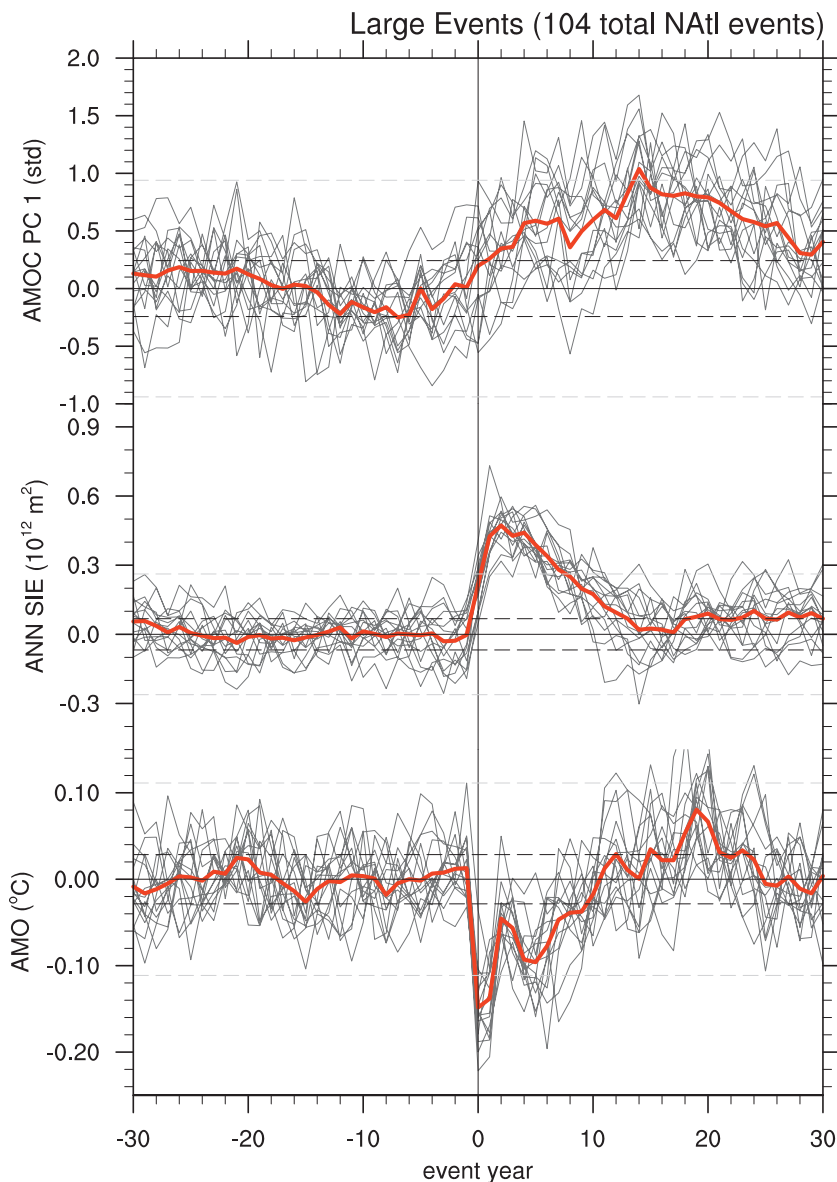


FIG. 12. Lead-lag relationships of AMOC leading-order principal component (PCI), NH annual SIE, and AMO composite responses to seven volcanic events with the largest impacts on annual radiation in the North Atlantic (greater than -10 W m^{-2} reduction in solar flux) for CESM-LME all-forcing and volcanic-only simulations. Composites for individual simulations (the ensemble of simulations) are shown by thin black (thick red) lines. The response is shown as a deviation from the 30-yr mean prior to the event. Year 0 is the first year of reduction in solar flux. Dashed lines represent two standard deviations for individual (light gray) and ensemble (black) bootstrap random events. The AMOC is represented with the leading-order PC time series and EOF analysis for 33°S – 60°N .

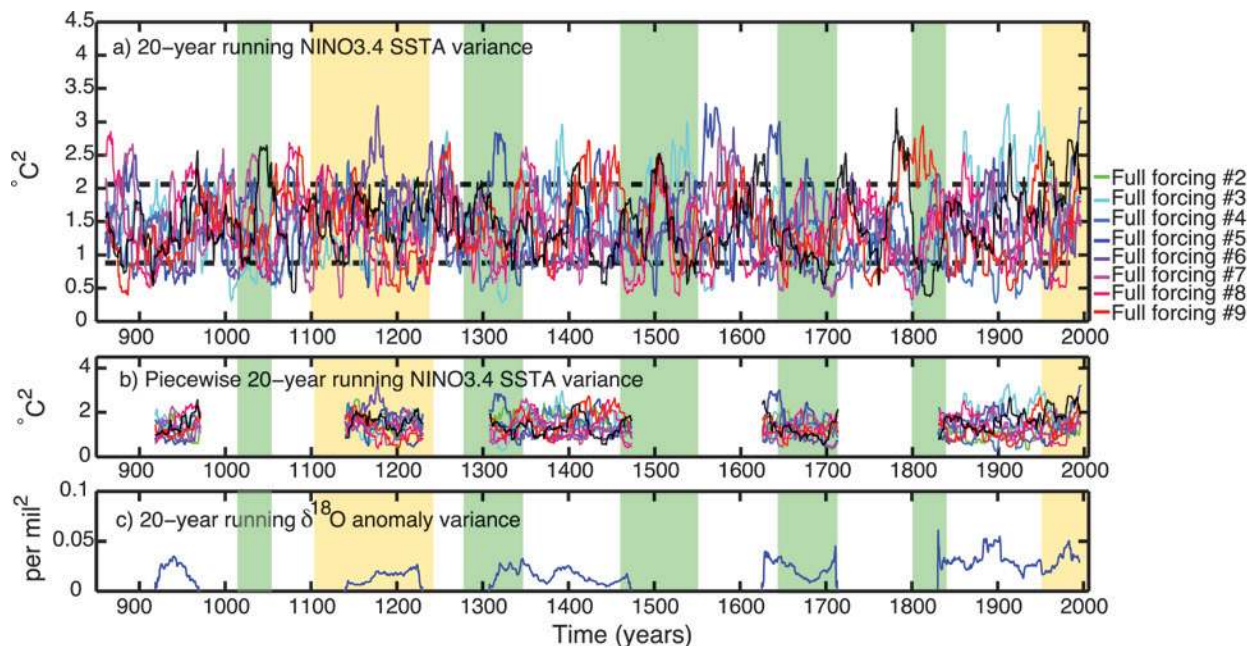


FIG. 13. Analyses of modulations in ENSO variability over the LM. (a) The 20-yr running Niño-3.4 variance ($^{\circ}\text{C}^2$) computed from the full-forcing CESM-LME simulations; green- and yellow-shaded regions indicate periods of minima and maxima in solar insolation, respectively. Horizontal dashed lines show the 10th and 90th percentiles of Niño-3.4 variance from the 850 control simulation. (b) Same variance data as in (a), but plotted only over time periods for which coral proxy data have been collected. (c) Variance (per mil²; %) of coral oxygen isotope records ($\delta^{18}\text{O}$) from a stacked time series, constructed using data from Palmyra Atoll in the North Pacific (Cobb et al. 2003), Maiana Atoll (Urban et al. 2000) and Tarawa (Cole et al. 1993) in Kiribati, Nauru (Guilderson and Schrag 1999), and Christmas Island in the Indian Ocean (McGregor et al. 2011).

Pongratz et al. (2008) reconstructions. New volcanic reconstructions incorporating additional records and better dating suggest that volcanic aerosol loading for some of the largest eruptions [e.g., Samalas (1257) and Kuwae (1453)] may have been overestimated by 20%–50%, and others underestimated by 20%–50% (Sigl et al. 2014). In addition, the magnitude of solar variability is still debated (Schmidt et al. 2012; Schurer et al. 2014). We plan to complete additional simulations to more fully explore the role of the uncertainties in the reconstructed forcings.

Our simulations do not include the “top down” effect of solar variability (Meehl et al. 2009). Simulations with the high-top chemistry version of CESM, the Whole Atmosphere Community Climate Model (WACCM5), are being run to explore the climatic responses to the stratospheric ozone changes to the solar intensity variations. New capabilities in CESM1 (Hurrell et al. 2013) will allow us to repeat earlier modeling studies on climate and carbon cycle dynamics over the last millennium (Jungclaus et al. 2010; Lehner et al. 2015), conduct CESM1 experiments that directly simulate the stable water isotopes measured in the proxies, and calculate the surface mass balance of the Greenland Ice Sheet.

This paper provides a few examples of the responses of CESM1(CAM5) to the natural and anthropogenic forcings from 850 to 2005. For further analyses by the community, the CESM-LME outputs are publicly available via the Earth System Grid (www.earthsystemgrid.org) as single variable time series in self-documenting loss-less compressed Network Common Data Form (NetCDF-4) format. High-frequency output for regional modeling and analysis of extremes is available for ensemble member 7 of the full-forcing simulations. The CESM-LME web page (www2.cesm.ucar.edu/models/experiments/LME) provides more background on the CESM-LME project, including diagnostic plots, lists of publications and ongoing projects, and instructions for reproducing the simulations.

ACKNOWLEDGMENTS. We thank the community of scientists and software engineers who have been instrumental in the development of CESM. The CESM project is supported by the National Science Foundation and the Office of Science (Biological and Environmental Research program) of the U.S. Department of Energy. JF and SS are supported by NSF EaSM2 Award AGS 1243107. LL is supported by the NOAA Climate Program Office

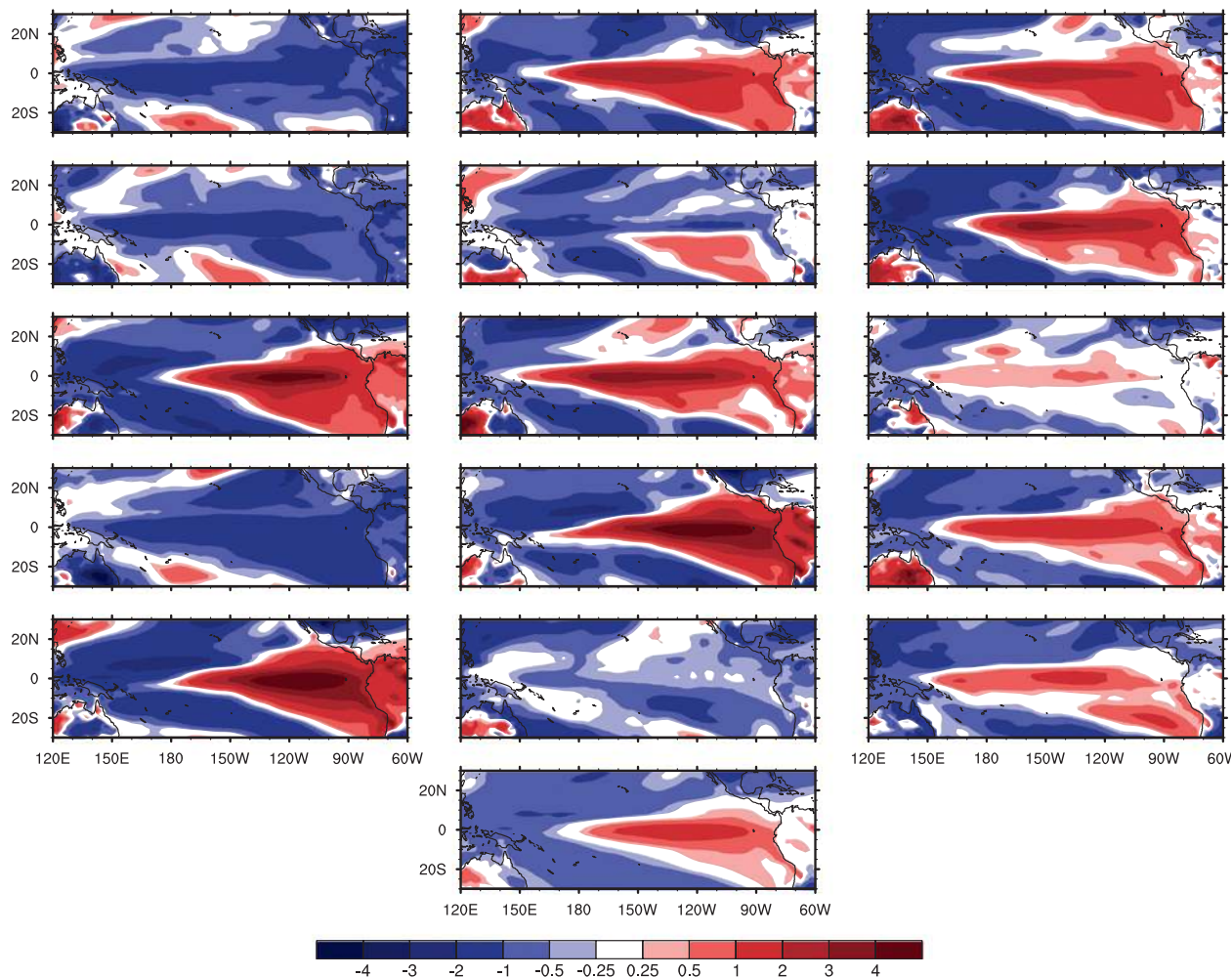


FIG. 14. TAMBORA eruption (Apr 1815) and the simulated tropical Pacific surface temperature anomalies ($^{\circ}\text{C}$) during winter 1816 for the 15 CESM-LME simulations that include volcanic forcing (top five rows) and the mean of these simulations (bottom row). The Dec–Feb (DJF) seasonal surface temperature anomalies for each simulation with volcanic forcing shown here are computed relative to each simulation’s long-term annual cycle.

under Climate Variability and Predictability Program Grant NA13OAR4310138. Computing resources were provided by the Climate Simulation Laboratory at NCAR’s Computational and Information Systems Laboratory (CISL) sponsored by the National Science Foundation and other agencies. Paleoclimatology data were downloaded from the World Data Center for Paleoclimatology operated by the NOAA/National Geophysical Data Center.

REFERENCES

- Adams, J. B., M. E. Mann, and C. Ammann, 2003: Proxy evidence for an El Niño-like response to volcanic forcing. *Nature*, **426**, 274–278, doi:10.1038/nature02101.
- Ammann, C. M., and E. R. Wahl, 2007: The importance of the geophysical context in statistical evaluations of climate reconstruction procedures. *Climatic Change*, **85**, 71–88, doi:10.1007/s10584-007-9276-x.
- Andres, H. J., and W. R. Peltier, 2013: Examining internal and external contributors to Greenland climate variability using CCSM3. *J. Climate*, **26**, 9745–9773, doi:10.1175/JCLI-D-12-00845.1.
- Berger, A. L., 1978: Long-term variations of daily insolation and Quaternary climatic changes. *J. Atmos. Sci.*, **35**, 2362–2367, doi:10.1175/1520-0469(1978)035<2362:LTVODI>2.0.CO;2.
- Bindoff, N. L., and Coauthors, 2013: Detection and attribution of climate change: From global to regional. *Climate Change 2013: The Physical Science Basis*, T. F. Stocker et al., Eds., Cambridge University Press, 867–952.
- Bothe, O., J. H. Jungclauss, and D. Zanchettin, 2013: Consistency of the multi-model CMIP5/

- PMIP3-past1000 ensemble. *Climate Past*, **9**, 2471–2487, doi:10.5194/cp-9-2471-2013.
- Bradley, R. S., M. K. Hughes, and H. F. Diaz, 2003: Climate in medieval time. *Science*, **302**, 404–405, doi:10.1126/science.1090372.
- Briffa, K. R., 2000: Annual climate variability in the Holocene: Interpreting the message of ancient trees. *Quat. Sci. Rev.*, **19**, 87–105, doi:10.1016/S0277-3791(99)00056-6.
- Cavalieri, D. J., and C. L. Parkinson, 2012: Arctic sea ice variability and trends, 1979–2010. *Cryosphere*, **6**, 881–889, doi:10.5194/tc-6-881-2012.
- Coats, S., B. I. Cook, J. S. Smerdon, and R. Seager, 2015: North American pancontinental droughts in model simulations of the last millennium. *J. Climate*, **28**, 2025–2043, doi:10.1175/JCLI-D-14-00634.1.
- Cobb, K. M., C. D. Charles, H. Cheng, and R. L. Edwards, 2003: El Niño/Southern Oscillation and tropical Pacific climate during the last millennium. *Nature*, **424**, 271–276, doi:10.1038/nature01779.
- , N. Westphal, H. R. Sayani, J. T. Watson, E. Di Lorenzo, H. Cheng, R. L. Edwards, and C. D. Charles, 2013: Highly variable El Niño–Southern Oscillation throughout the Holocene. *Science*, **339**, 67–70, doi:10.1126/science.1228246.
- Cole, J. E., R. G. Fairbanks, and G. T. Shen, 1993: The spectrum of recent variability in the Southern Oscillation: Results from a Tarawa Atoll coral. *Science*, **260**, 1790–1793, doi:10.1126/science.260.5115.1790.
- Collins, M., and Coauthors, 2010: The impact of global warming on the tropical Pacific and El Niño. *Nat. Geosci.*, **3**, 391–397, doi:10.1038/ngeo868.
- Cook, B. I., T. R. Ault, and J. E. Smerdon, 2015: Unprecedented 21st century drought risk in the American Southwest and Central Plains. *Sci. Adv.*, **1**, e1400082, doi:10.1126/sciadv.1400082.
- Cook, E. R., D. M. Meko, D. W. Stahle, and M. K. Cleaveland, 1999: Drought reconstructions for the continental United States. *J. Climate*, **12**, 1145–1162, doi:10.1175/1520-0442(1999)012<1145:DRFTCU>2.0.CO;2.
- , C. A. Woodhouse, C. M. Eakin, D. M. Meko, and D. W. Stahle, 2004: Long-term aridity changes in the western United States. *Science*, **306**, 1015–1018, doi:10.1126/science.1102586.
- , B. M. Buckley, J. G. Palmer, P. Fenwick, M. J. Peterson, G. Boswijk, and A. Fowler, 2006: Millennia-long tree-ring records from Tasmania and New Zealand: A basis for modelling climate variability and forcing, past, present and future. *J. Quat. Sci.*, **21**, 689–699, doi:10.1002/jqs.1071.
- , K. J. Anchukaitis, B. M. Buckley, R. D. D’Arrigo, G. C. Jacoby, and W. E. Wright, 2010: Asian monsoon failure and megadrought during the last millennium. *Science*, **328**, 486–489, doi:10.1126/science.1185188.
- Crowley, T. J., and M. B. Unterman, 2013: Technical details concerning development of a 1200 yr proxy index for global volcanism. *Earth Syst. Sci. Data*, **5**, 187–197, doi:10.5194/essd-5-187-2013.
- Danabasoglu, G. D., S. G. Yeager, J. T. Tribbia, A. S. Phillips, and J. W. Hurrell, 2012: Variability of the Atlantic meridional overturning circulation in CCSM4. *J. Climate*, **25**, 5153–5172, doi:10.1175/JCLI-D-11-00463.1.
- Delworth, T. L., and M. E. Mann, 2000: Observed and simulated multidecadal variability in the Northern Hemisphere. *Climate Dyn.*, **16**, 661–676, doi:10.1007/s003820000075.
- Diaz, H. F., R. M. Trigo, M. K. Hughes, M. E. Mann, E. Xoplaki, and D. Barriopedro, 2011: Spatial and temporal characteristics of climate in medieval times revisited. *Bull. Amer. Meteor. Soc.*, **92**, 1487–1500, doi:10.1175/BAMS-D-10-05003.1.
- Eddy, J. A., 1976: The Maunder minimum. *Science*, **192**, 1189–1202, doi:10.1126/science.192.4245.1189.
- Fernández-Donado, L., and Coauthors, 2013: Temperature response to external forcing in simulations and reconstructions of the last millennium. *Climate Past*, **9**, 393–421, doi:10.5194/cp-9-393-2013.
- Flato, G., and Coauthors, 2013: Evaluation of climate models. *Climate Change 2013: The Physical Science Basis*, T. F. Stocker et al., Eds., Cambridge University Press, 741–866.
- Fritts, H. C., G. R. Lofgren, and G. A. Gordon, 1979: Variations in climate since 1602 as reconstructed from tree rings. *Quat. Res.*, **12**, 18–46, doi:10.1016/0033-5894(79)90090-5.
- Gao, C., A. Robock, and C. Ammann, 2008: Volcanic forcing of climate over the last 1500 years: An improved ice core–based index for climate models. *J. Geophys. Res.*, **113**, D23111, doi:10.1029/2008JD010239.
- Gent, P. R., and Coauthors, 2011: The Community Climate System Model Version 4. *J. Climate*, **24**, 4973–4991, doi:10.1175/2011JCLI4083.1.
- Goosse, H., H. Renssen, A. Timmermann, and R. S. Bradley, 2005: Internal and forced climate variability during the last millennium: A model–data comparison using ensemble simulations. *Quat. Sci. Rev.*, **24**, 1345–1360, doi:10.1016/j.quascirev.2004.12.009.
- Graf, W., H. Oerter, O. Reinwarth, W. Stichler, F. Wilhelms, H. Miller, and R. Mulvaney, 2002: Stable isotope records from Dronning Maud Land, Antarctica. *Ann. Glaciol.*, **35**, 195–201, doi:10.3189/172756402781816492.

- Guilderson, T. P., and D. P. Schrag, 1999: Reliability of coral isotope records from the western Pacific warm pool: A comparison using age-optimized records. *Paleoceanography*, **14**, 457–464, doi:10.1029/1999PA900024.
- Handler, P., 1984: Possible association of stratospheric aerosols and El Niño type events. *Geophys. Res. Lett.*, **11**, 1121–1124, doi:10.1029/GL011i011p01121.
- Hansen, J., R. Ruedy, M. Sato, and K. Lo, 2010: Global surface temperature. *Rev. Geophys.*, **48**, RG4004, doi:10.1029/2010RG000345.
- He, F., S. J. Vavrus, J. E. Kutzbach, W. F. Ruddiman, J. O. Kaplan, and K. M. Krumhardt, 2014: Simulating global and local surface temperature changes due to Holocene anthropogenic land cover change. *Geophys. Res. Lett.*, **41**, 623–631, doi:10.1002/2013GL058085.
- Hurrell, J., and Coauthors, 2013: The Community Earth System Model: A framework for collaborative research. *Bull. Amer. Meteor. Soc.*, **94**, 1339–1360, doi:10.1175/BAMS-D-12-00121.1.
- Hurttt, G. C., and Coauthors, 2011: Harmonization of land-use scenarios for the period 1500–2100: 600 years of global gridded annual land-use transitions, wood harvest, and resulting secondary lands. *Climatic Change*, **109**, 117–161, doi:10.1007/s10584-011-0153-2.
- Jansen, E., and Coauthors, 2007: Paleoclimate. *Climate Change 2007: The Physical Science Basis*, S. Solomon et al., Eds., Cambridge University Press, 433–497.
- Jones, P. D., and Coauthors, 2009: High-resolution palaeoclimatology of the last millennium: A review of current status and future prospects. *Holocene*, **19**, 3–49, doi:10.1177/0959683608098952.
- Juckes, M. N., and Coauthors, 2007: Millennial temperature reconstruction intercomparison and evaluation. *Climate Past*, **3**, 591–609, doi:10.5194/cp-3-591-2007.
- Jungclauss, J. H., S. J. Lorenz, C. Timmreck, C. H. Reick, V. Brovkin, K. Six, and J. Marotzke, 2010: Climate and carbon-cycle variability over the last millennium. *Climate Past*, **6**, 723–737, doi:10.5194/cp-6-723-2010.
- Kaplan, J. O., K. M. Krumhardt, E. C. Ellis, W. F. Ruddiman, C. Lemmen, and K. Klein Goldewijk, 2011: Holocene carbon emissions as a result of anthropogenic land cover change. *Holocene*, **21**, 775–791, doi:10.1177/0959683610386983.
- Kaufman, D. S., and Coauthors, 2009: Recent warming reverses long-term Arctic cooling. *Science*, **325**, 1236–1239, doi:10.1126/science.1173983.
- Kay, J. E., and Coauthors, 2015: The Community Earth System Model (CESM) Large Ensemble Project: A community resource for studying climate change in the presence of internal variability. *Bull. Amer. Meteor. Soc.*, **96**, 1333–1349, doi:10.1175/BAMS-D-13-00255.1.
- Kemp, M., 2008: Looking at the face of the Earth. *Nature*, **456**, 876, doi:10.1038/456876a.
- Kinnard, C., C. M. Zdanowicz, D. A. Fisher, E. Isaksson, A. de Vernal, and L. G. Thompson, 2011: Reconstructed changes in Arctic sea ice over the past 1,450 years. *Nature*, **479**, 509–512, doi:10.1038/nature10581.
- Knudsen, M. F., M.-S. Seidenkrantz, B. H. Jacobsen, and A. Kuijpers, 2011: Tracking the Atlantic multi-decadal oscillation through the last 8,000 years. *Nat. Commun.*, **2**, 178, doi:10.1038/ncomms1186.
- Landrum, L., B. L. Otto-Bliesner, E. R. Wahl, A. Conley, P. J. Lawrence, and H. Teng, 2013: Last millennium climate and its variability in CCSM4. *J. Climate*, **26**, 1085–1111, doi:10.1175/JCLI-D-11-00326.1.
- Lean, J. L., 2010: Cycles and trends in solar irradiance and climate. *Wiley Interdiscip. Rev.: Climate Change*, **1**, 111–122, doi:10.1002/wcc.18.
- Lehner, F., A. Born, C. R. Raible, and T. F. Stocker, 2013: Amplified inception of European Little Ice Age by sea ice–ocean–atmosphere feedbacks. *J. Climate*, **26**, 7586–7602, doi:10.1175/JCLI-D-12-00690.1.
- , F. Joos, C. C. Raible, J. Mignot, A. Born, K. M. Keller, and T. F. Stocker, 2015: Climate and carbon cycle dynamics in a CESM simulation from 850–2100 CE. *Earth Syst. Dyn.*, **6**, 411–434, doi:10.5194/esdd-6-351-2015.
- Li, J., S.-P. Xie, E. R. Cook, G. Huang, R. D’Arrigo, F. Liu, J. Ma, and X.-T. Zheng, 2011: Interdecadal modulation of El Niño amplitude during the past millennium. *Nat. Climate Change*, **1**, 114–118, doi:10.1038/nclimate1086.
- Loehle, C., and J. H. McCulloch, 2008: Correction to: A 2000-year global temperature reconstruction based on non-tree ring proxies. *Energy Environ.*, **19**, 93–100, doi:10.1260/095830508783563109.
- Mann, M. E., Z. Zhang, M. K. Hughes, R. S. Bradley, S. K. Miller, S. Rutherford, and F. Ni, 2008: Proxy-based reconstructions of hemispheric and global surface temperature variations over the past two millennia. *Proc. Natl. Acad. Sci. USA*, **105**, 13252–13257, doi:10.1073/pnas.0805721105.
- , and Coauthors, 2009: Global signatures and dynamical origins of the Little Ice Age and Medieval Climate Anomaly. *Science*, **326**, 1256–1260, doi:10.1126/science.1177303.
- Massé, G., S. J. Rowland, M.-A. Sicre, J. Jacob, E. Jansen, and S. T. Belt, 2008: Abrupt climate changes for Iceland during the last millennium: Evidence from high resolution sea ice reconstructions. *Earth Planet. Sci. Lett.*, **269**, 565–569, doi:10.1016/j.epsl.2008.03.017.
- Masson-Delmotte, V., and Coauthors, 2013: Information from paleoclimate archives. *Climate Change 2013:*

- The Physical Science Basis*, T. F. Stocker et al., Eds., Cambridge University Press, 383–464.
- McGregor, H. V., M. J. Fischer, M. K. Gagan, D. Fink, and C. D. Woodroffe, 2011: Environmental control of the oxygen isotope composition of Porites coral microatolls. *Geochim. Cosmochim. Acta*, **75**, 3930–3944, doi:10.1016/j.gca.2011.04.017.
- McGregor, S., A. Timmermann, and O. Timm, 2010: A unified proxy for ENSO and PDO variability since 1650. *Climate Past*, **6**, 1–17, doi:10.5194/cp-6-1-2010.
- Meehl, G. A., J. M. Arblaster, K. Matthes, F. Sassi, and H. van Loon, 2009: Amplifying the Pacific climate system response to a small 11-year solar cycle forcing. *Science*, **325**, 1114–1118, doi:10.1126/science.1172872.
- , and Coauthors, 2012: Climate system response to external forcings and climate change projections in CCSM4. *J. Climate*, **25**, 3661–3683, doi:10.1175/JCLI-D-11-00240.1.
- Miller, G. H., and Coauthors, 2012: Abrupt onset of the Little Ice Age triggered by volcanism and sustained by sea-ice/ocean feedbacks. *Geophys. Res. Lett.*, **39**, L02708, doi:10.1029/2011GL050168.
- Moberg, A., D. M. Sonechkin, K. Holmgren, N. M. Datsenko, and W. Karlén, 2005: Highly variable Northern Hemisphere temperatures reconstructed from low- and high-resolution proxy data. *Nature*, **433**, 613–617, doi:10.1038/nature03265.
- Morice, C. P., J. J. Kennedy, N. A. Rayner, and P. D. Jones, 2012: Quantifying uncertainties in global and regional temperature change using an ensemble of observational estimates: The HadCRUT4 data set. *J. Geophys. Res.*, **117**, D08101, doi:10.1029/2011JD017187.
- Ottera, O. H., M. Bentsen, H. Drange, and L. L. Suo, 2010: External forcing as a metronome for Atlantic multidecadal variability. *Nat. Geosci.*, **3**, 688–694, doi:10.1038/ngeo955.
- PAGES 2k Consortium, 2013: Continental-scale temperature variability during the last two millennia. *Nat. Geosci.*, **6**, 339–346, doi:10.1038/ngeo1797.
- Phipps, S. A., and Coauthors, 2013: Paleoclimate data-model comparison and the role of climate forcings over the past 1500 years. *J. Climate*, **26**, 6915–6936, doi:10.1175/JCLI-D-12-00108.1.
- Pongratz, J., C. H. Reick, T. Raddatz, and M. Claussen, 2008: A reconstruction of global agricultural areas and land cover for the last millennium. *Global Biogeochem. Cycles*, **22**, GB3018, doi:10.1029/2007GB003153.
- Robock, A., 2000: Volcanic eruptions and Climate. *Rev. Geophys.*, **38**, 191–219, doi:10.1029/1998RG000054.
- Scafetta, N., and B. J. West, 2008: Is climate sensitive to solar variability? *Phys. Today*, **61**, 50–51, doi:10.1063/1.2897951.
- Schmidt, G. A., and Coauthors, 2011: Climate forcing reconstructions for use in PMIP simulations of the Last Millennium (v1.0). *Geosci. Model Dev.*, **4**, 33–45, doi:10.5194/gmd-4-33-2011.
- , and Coauthors, 2012: Climate forcing reconstructions for use in PMIP simulations of the Last Millennium (v1.1). *Geosci. Model Dev.*, **5**, 185–191, doi:10.5194/gmd-5-185-2012.
- , and Coauthors, 2014: Using palaeo-climate comparisons to constrain future projections in CMIP5. *Climate Past*, **10**, 221–250, doi:10.5194/cp-10-221-2014.
- Schurer, A. P., G. C. Hegerl, M. E. Mann, S. F. B. Tett, and S. J. Phipps, 2013: Separating forced from chaotic climate variability over the past millennium. *J. Climate*, **26**, 6954–6973, doi:10.1175/JCLI-D-12-00826.1.
- , S. F. B. Tett, and G. C. Hegerl, 2014: Small influences of solar variability on climate over the past millennium. *Nat. Geosci.*, **7**, 104–108, doi:10.1038/ngeo2040.
- Self, S., M. R. Rampino, J. Zhao, and M. G. Katz, 1997: Volcanic aerosol perturbations and strong El Niño events: No general correlation. *Geophys. Res. Lett.*, **24**, 1247–1250, doi:10.1029/97GL01127.
- Sigl, M., and Coauthors, 2014: Insights from Antarctica on volcanic forcing during the Common Era. *Nat. Climate Change*, **4**, 693–697, doi:10.1038/nclimate2293.
- Stommel, H. M., and E. Stommel, 1983: *Volcano Weather: The Story of 1816, The Year without a Summer*. Seven Seas Press, 177 pp.
- Stothers, R. B., 1984: The great Tambora eruption in 1815 and its aftermath. *Science*, **224**, 1191–1198, doi:10.1126/science.224.4654.1191.
- Stroeve, J., M. Serreze, S. Drobot, S. Gearheard, M. Holland, J. Maslanik, W. Meier, and T. Scambos, 2008: Arctic sea ice extent plummets in 2007. *Eos, Trans. Amer. Geophys. Union*, **89**, 13–14, doi:10.1029/2008EO020001.
- Swart, N. C., J. C. Fyfe, E. Hawkins, J. E. Kay, and A. Jahn, 2015: Influence of internal variability on Arctic sea-ice trends. *Nat. Climate Change*, **5**, 86–89, doi:10.1038/nclimate2483.
- Taylor, K. E., R. J. Stouffer, and G. A. Meehl, 2012: An overview of CMIP5 and the experiment design. *Bull. Amer. Meteor. Soc.*, **93**, 485–498, doi:10.1175/BAMS-D-11-00094.1.
- Trouet, V., J. Esper, N. E. Graham, A. Baker, J. D. Scourse, and D. C. Frank, 2009: Persistent positive North Atlantic oscillation mode dominated the

- Medieval Climate Anomaly. *Science*, **324**, 78–80, doi:10.1126/science.1166349.
- Turner, J., T. J. Bracegirdle, T. Phillips, G. J. Marshall, and J. S. Hosking, 2013: An initial assessment of Antarctic sea ice extent in the CMIP5 models. *J. Climate*, **26**, 1473–1484, doi:10.1175/JCLI-D-12-00068.1.
- Urban, F. E., J. E. Cole, and J. T. Overpeck, 2000: Influence of mean climate change on climate variability from a 155-year tropical Pacific coral record. *Nature*, **407**, 989–993, doi:10.1038/35039597.
- Vieira, L. E. A., S. K. Solanki, N. A. Krivova, and I. Usoskin, 2011: Evolution of the solar irradiance during the Holocene. *Astron. Astrophys.*, **531**, A6, doi:10.1051/0004-6361/201015843.
- Vinther, B. M., and Coauthors, 2009: Holocene thinning of the Greenland Ice Sheet. *Nature*, **461**, 385–388, doi:10.1038/nature08355.
- Wahl, E. R., H. F. Diaz, J. E. Smerdon, and C. M. Ammann, 2014: Late winter temperature response to large tropical volcanic eruptions in temperate western North America: Relationship to ENSO phases. *Global Planet. Change*, **122**, 238–250, doi:10.1016/j.gloplacha.2014.08.005.
- Wang, Y., and Coauthors, 2005: The Holocene Asian monsoon and links to the solar changes and North Atlantic climate. *Science*, **308**, 854–857, doi:10.1126/science.1106296.
- Woodhouse, C. A., and J. T. Overpeck, 1998: 2000 years of drought variability in the central United States. *Bull. Amer. Meteor. Soc.*, **79**, 2693–2714, doi:10.1175/1520-0477(1998)079<2693:YODVIT>2.0.CO;2.
- Wuebbles, D., and Coauthors, 2014: CMIP5 climate model analyses: Climate extremes in the United States. *Bull. Amer. Meteor. Soc.*, **95**, 571–583, doi:10.1175/BAMS-D-12-00172.1.
- Zhong, Y., G. H. Miller, B. L. Otto-Bliesner, M. M. Holland, D. A. Bailey, D. P. Schneider, and A. Geirsdottir, 2011: Centennial-scale climate change from decadal-paced explosive volcanism: A coupled sea ice-ocean mechanism. *Climate Dyn.*, **37**, 2373–2387, doi:10.1007/s00382-010-0967-z.

NEW FROM AMS BOOKS!

The Thinking Person's Guide to Climate Change

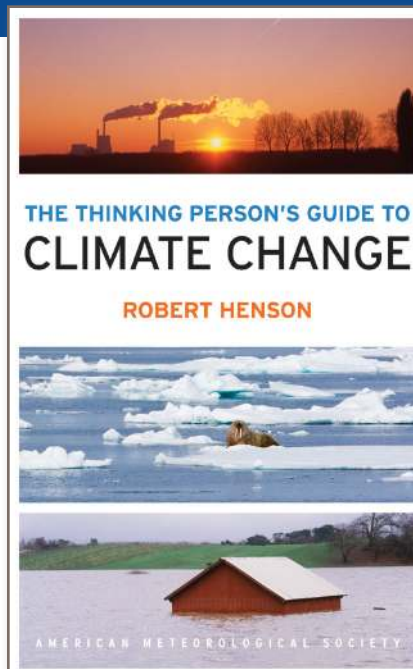
Robert Henson

Expanded and updated from Henson's *Rough Guide to Climate Change*, 3rd edition (no longer in print), combining years of data with recent research, including conclusions from the Fifth Assessment Report of the Intergovernmental Panel on Climate Change, the Guide breaks down the issues into straightforward categories:

- Symptoms, including melting ice and extreme weather
- Science, laying out what we know and how we know it
- Debates, tackling the controversy and politics
- Solutions and Actions for creating the best possible future

© 2014, 516 pages, paperback
ISBN: 978-1-878220-73-7

List price: \$30 AMS Member price: \$20



AMS BOOKS

RESEARCH APPLICATIONS HISTORY

➤ bookstore.ametsoc.org